

HARPA: High-Rate Phase Association with Travel Time Neural Fields

Cheng Shi¹, Maarten V. de Hoop², and Ivan Dokmanić^{1,3}

¹*Departement of Mathematics and Computer Science, University of Basel*

²*Simons Chair in Computational and Applied Mathematics and Earth Science, Rice University*

³*Department of ECE, University of Illinois at Urbana–Champaign*

July 18, 2023

Abstract

Phase association groups seismic wave arrivals according to their originating earthquakes. It is a fundamental task in a seismic data processing pipeline, but challenging to perform for smaller, high-rate seismic events which carry fundamental information about earthquake dynamics, especially with a commonly assumed inaccurate wave speed model. As a consequence, most association methods focus on larger events that occur at a lower rate and are thus easier to associate, even though microseismicity provides a valuable description of the elastic medium properties in the subsurface. In this paper, we show that association is possible at rates much higher than previously reported even when the wave speed is unknown. We propose HARPA, a high-rate seismic phase association method which leverages deep neural fields to build generative models of wave speeds and associated travel times, and first solves a joint spatio-temporal source localization and wave speed recovery problem, followed by association. We obviate the need for associated phases by interpreting arrival time data as probability measures and using an optimal transport loss to enforce data fidelity. The joint recovery problem is known to admit a unique solution under certain conditions but due to the non-convexity of the corresponding loss a simple gradient scheme converges to poor local minima. We show that this is effectively mitigated by stochastic gradient Langevin dynamics (SGLD). Numerical experiments show that HARPA efficiently associates high-rate seismicity clouds over complex, unknown wave speeds and graciously handles noisy and missing picks.

1 Introduction

Seismic signals carry valuable information about the structure and dynamics of the Earth and other planets. A standard processing pipeline begins with identifying wave arrivals and their types. In travel-time tomography the essential attribute of a seismic wave is its arrival time at the receivers. If we know the wave speed, we can use the arrival times to determine source locations in space and time. Multiple sources may enable us to estimate the wave speed itself but this usually requires that we can group the arrivals at different stations which correspond to the same events.

This grouping or *phase association problem* is straightforward to solve when the events and their selected phases are sufficiently separated in time (middle panel in Figure 1); one can ensure that this holds by concentrating on large, infrequent events such as major earthquakes. A challenge emerges in regions of high seismicity or when attempting to use smaller, more frequent events (right panel in Figure 1). Such micro-seismic events may enable a much better understanding of the spatial

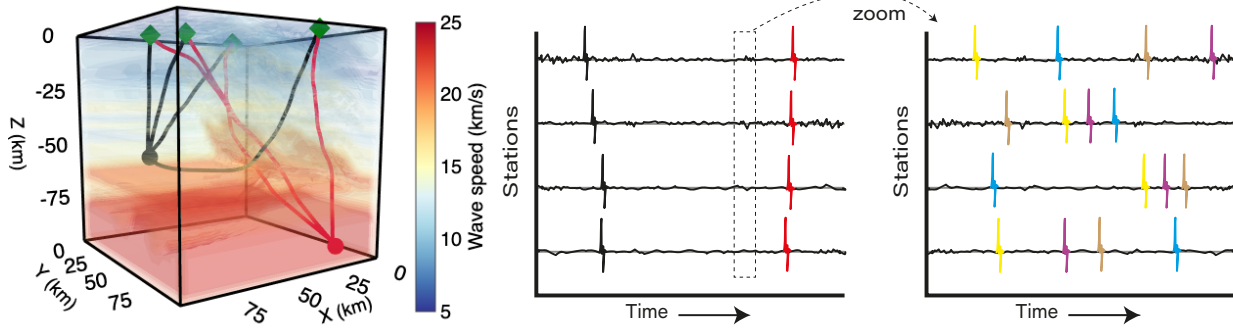


Figure 1: Illustration of the seismic association problem. Left: rays corresponding to seismic waves propagate in an inhomogeneous medium; middle: a sample of recorded seismic data, scaled to emphasize intense events; right: observed seismic data scaled to emphasize small but frequent events. Phases of same color originate from the same source.

variability of elastic material properties within the crust and upper mantle, but these events are hard to use in traditional pipelines due to the inefficiency of existing association algorithms. There are currently no algorithms that can perform association reliably in the highly-interleaved regime where waves from many seismic events arrive topsy-turvy at the stations at similar times. The problem is challenging even when the wave speed is known. In many regions, however, the wave speed is not known at the resolution required, or, at best, only a rough approximation is available. It is thus paramount to develop methods that can handle the related uncertainty.

To address this gap we propose HARPA—a method that can solve the high-rate association problem over an unknown wave speed in settings considerably more complex than attainable by existing methods. HARPA first solves a seemingly harder problem: estimating locations and occurrence times of earthquakes jointly with an (approximate) wave speed model. Only then does it assign earthquake phases, but with the approximately known earthquake and wave speed parameters the problem again becomes a simple linear assignment problem. This simplification is afforded by leveraging the physics of wave propagation.

The described procedure may seem to contradict our earlier statement that source localization relies on *associated* phases. While this is indeed a prerequisite for the traditional localization methods, we obviate the need for associated phases by interpreting the arrival time data at each station as a probability measure. We then minimize the optimal transport distance between measures corresponding to the observed data and those produced by our estimates of earthquake parameters and the wave speed.

There are two major challenges in implementing this program. The first is to enable numerically efficient differentiable optimization with respect to source locations and wave speed models which respects propagation physics. This is all but impossible with traditional mesh-based eikonal solvers. Even if we devise a way to do it, scaling to 3D would result in prohibitive computational complexity. The second challenge lies in finding the globally optimal solution of the associated non-convex optimization problem. While the problem of wave speed reconstruction from unknown sources admits a unique solution under certain conditions [7], identifying this solution by optimizing a non-convex objective is challenging due to the presence of poor local minima. A standard gradient descent algorithm generally converges to local rather global minima.

To resolve the first challenge, we first train a deep generative model to embed a family of complex wave speeds in a low-dimensional latent space and optimize the latent code of the wave speed and

the spatio-temporal earthquake parameters simultaneously. But instead of directly addressing the formidable challenge of optimizing these parameters through a numerical solver we train a deep neural field to fit the travel times between arbitrary interior points and a fixed set of receivers. An autoencoder structures the latent space and provides a pairing between latent codes and wave speeds which is then used by the travel time neural field. As we show in Section 4, fitting the best wave speed from the range of a sufficiently diverse generative model provides significant robustness in association, even when the test wave speed is out of the distribution used to train the model.

To resolve the second challenge, we leverage a combination of stochastic gradient-based methods and sampling: Markov Chain Monte Carlo (MCMC) methods can in principle deal with the non-convexity but they are ineffective as the search space in our setting is too large. We employ Stochastic Gradient Langevin Dynamics (SGLD) [37] to ensure adequate exploration of the loss landscape by the gradient optimizer, ultimately leading to the identification of the global minimum. We further demonstrate that HARPA remains robust in the face of reasonable wave speed distortions, as well as noisy or missing arrival picks at the stations.

We test HARPA on a suite of challenging computer experiments, on complex unknown wave speeds and with extremely dense seismic events which arrive at different stations in completely different sequences. We demonstrate for the first time accurate and robust phase association in this regime, suggesting exciting new avenues in exploratory Earth science.

All results in this paper are fully reproducible; code at https://github.com/DaDaCheng/phase_association.

1.1 Related work

1.1.1 Combinatorial optimization

If earthquake source locations, occurrence times, and wave speeds are all known, the phase association problem can be formulated as a linear sum assignment problem (LSAP), which is effectively solved by the Hungarian algorithm [6]. If only the occurrence times are unknown, the problem is related to a quadratic assignment problem (QAP) [16, 27] which is NP-hard. While QAPs can be solved in certain practical cases using heuristics and meta-heuristics [2, 5], there has been growing interest in leveraging machine learning to solve similar combinatorial optimization problems [18, 26, 36]. The situation, however, is often even more complex: neither the wave speed nor the spatiotemporal earthquake source locations are known, although sometimes a rather coarse wave speed model is available. These unknown degrees of freedom result in a mixed-integer programming problem which is harder than an LSAP or a QAP and challenging to solve even with a small number of earthquakes and stations.

1.1.2 Inverse problems in Riemannian geometry

The joint localization–wave speed recovery problem has a unique solution under certain conditions [7]; there are, however, no reliable algorithms that can provably solve it within reasonable time. Notwithstanding, on the algorithmic side there were attempts to perform joint full waveform (or sometimes travel time) inversion and wave speed model refinement but with temporally well-separated sources implicitly avoiding the association problem, while facing the ill-posedness. In the context of micro-seismicity, simple parametric models [14] and Bayesian priors [42] were used for regularization [34, 35, 38]. We mention that our strategy to convert combinatorial data into measures in order to avoid combinatorial optimization is reminiscent of earlier work on unassigned Euclidean distance data [8, 13] with applications in genomics and room acoustics.

1.1.3 Seismology and machine learning

There has been an increasing interest in the application of machine learning in seismology, for example for phase picking [43]. A multitude of studies addressing the phase association problem have employed either probabilistic [30, 31, 44] or graph models [22, 23]. These approaches demand large quantities of data for training. One reason for that is that they do not explicitly leverage the wave propagation physics. All phenomena in the association problem are governed by the wave equation which is known, but is typically only leveraged for downstream analysis once the phases have been associated. We show that rethinking the problem in measure-theoretic terms allows one to leverage the wave propagation model from the very beginning.

2 Problem formulation

We consider an unknown wave speed $c : \Omega \rightarrow \mathbb{R}^+$ where $\Omega \subset \mathbb{R}^3$ is the domain of interest that contains sources and ray paths. For a given c , we use $T_c(s; r)$ to represent the time it takes for a wave to travel from source point $s \in \Omega$ to a boundary receiver point $r \in \partial\Omega$. We assume there are N stations and M sources. Each source generates one event, and we assume that each station receives K phases originating from the M sources. (We first assume $K = M$ and later discuss situations with noisy and missing picks where $K \neq M$.) We let $\mathcal{R} = \{r_i \in \Omega \mid i \leq N\}$ be the set of the N stations locations. Arrival time data recorded at each station is denoted by $\mathcal{D}_i = \{t_{i,k} \mid k \leq M\}$, where $t_{i,k}$ represents the arrival time for each pick. For a given fixed time window, we observe earthquakes with spatio-temporal locations $\mathcal{E} = \{(s_j, \tau_j) \mid s_j \in \Omega, \tau_j \in [0, \tau_{\max}], j \leq M\}$. If an earthquake with location and occurrence time $e_j = (s_j, \tau_j)$ is observed as the k -th arrival at station i with arrival time $t_{i,k}$, we have

$$t_{i,k} = T_c(s_j; r_i) + \tau_j. \quad (1)$$

The goal of the source–receiver association is to determine which picks correspond to which source. To model this, we define the ground truth association as

$$\alpha^*(k; r_i) := j \leq M,$$

and its corresponding inverse assignment as

$$\alpha^{*-1}(j; r_i) := k \leq M.$$

2.1 A mixed-integer optimization problem

We aim to infer the assignment α^* (up to a global permutation), the unknown wave speed c^* , and source locations and times \mathcal{E}^* , from arrival time data. This can be formulated as the following mixed-integer optimization problem,

$$\underset{\alpha, c, \mathcal{E}}{\text{minimize}} \quad L(\alpha; c, \mathcal{E}), \quad (2)$$

where the loss function is defined using a suitable discrepancy metric $\ell(a, b)$ on the arrival times,

$$L(\alpha; c, \mathcal{E}) = \sum_{j \leq M, i \leq N} \ell(T_c(s_j; r_i) + \tau_j, t_{i, \alpha^{*-1}(j; r_i)}). \quad (3)$$

We mention in the passing that some works deal with the unknown occurrence times by using time difference of arrival (TDoA) data instead of including the takeoff times as optimization variables;

this is achieved by minimizing the mismatch loss

$$L^M(\alpha; c, \mathcal{E}) = \sum_{j \leq M, i_a < i_b \leq N} \ell \left(T_c(s_j; r_{i_a}) - T_c(s_j; r_{i_b}), t_{i_a, \alpha^{-1}(j; r_{i_a})} - t_{i_b, \alpha^{-1}(j; r_{i_b})} \right). \quad (4)$$

Since we also recover the takeoff times we work directly with ToAs.

2.1.1 Low dimensional wave speed families

To build HARPA we assume that the wave speed models and consequently travel times exhibit a latent low-dimensional structure. We thus model the wave speeds by an autoencoder-based generative model and traveltimes by a matching continuous coordinate-based neural field [24, 33, 39]. The assumption of latent low-dimensionality is consistent with geodynamical models generating the distribution of the elastic material properties in the interior; this has been explored for Earth's mantle before [25, 32]. In fact, the wave speeds generated by our latent model ($\mathbb{R}^L \ni z \mapsto c(z)$) are considerably more complex than the fixed models used for association in the recent literature which only vary along the depth coordinate [19, 31, 44]. We thus define the associated travel time function as $T(s, z; r) = T_c(s; r)$. This enables us to rewrite the optimization problem involving c as one involving the latent code z ,

$$\underset{\alpha, z, \mathcal{E}}{\text{minimize}} \quad L(\alpha; c(z), \mathcal{E}). \quad (5)$$

2.2 Characterizing the difficulty of the association problem

In order to characterize the hardness of joint inference and association problems, we define the *confusion factor* as

$$\begin{aligned} \text{CF} &= 1 - \max \left\{ \frac{1}{N} \sum_{i=1}^N \mathcal{T} \left[\{(T_c(s_j; r_i) + \tau_j, \tau_j)\}_{j=1}^M \right], 0 \right\} \\ &= 1 - \max \left\{ \frac{1}{N} \sum_{i=1}^N \mathcal{T} \left[\{(t_{i, \alpha^*(j; r_i)}, \tau_j)\}_{j=1}^M \right], 0 \right\}, \end{aligned} \quad (6)$$

where

$$\mathcal{T} \left[\{(a_j, b_j)\}_j \right] = \frac{\text{number of concordant pairs} - \text{number of discordant pairs}}{\text{number of pairs}}$$

calculates Kendall's τ rank correlation coefficient [15]. Succinctly, when the order of the arrivals at a station matches the order of earthquake occurrences, \mathcal{T} yields a value of 1 and $\text{CF} = 0$. This typically occurs during low-rate earthquakes, where the travel time is shorter than the time between the different events. Conversely, when all earthquakes occur almost simultaneously, the order of earthquake occurrence bears no correlation with the order of the phases/picks arriving at the stations. This reduces \mathcal{T} closer to 0, and pushes CF closer to 1, implying a higher level of confusion (the CF is always between 0 and 1). When studying regions such as Ridgecrest around the time of the 2019 earthquake, the magnitude cutoff is usually chosen so that the resulting CF is below 0.1 [29, 31, 44]. Figure 2 shows representative arrival configurations for different values of CF ; Figure 9 shows results of an exhaustive test of the proposed method at different CF .

The difficulty of association is not solely determined by CF ; it also depends on the number of stations N and the number of sources M being simultaneously associated. Many algorithms initially partition the data into shorter temporal windows, usually between 5 and 20 seconds in

length, with approximately 5 to 20 events in each window [43, 44]. In this proof of concept we focus on a single window.

To characterize performance we also record the phase association accuracy defined as

$$\text{ACC} = \frac{1}{NM} \sum_{i=1}^N \sum_{j=1}^M \delta(\alpha(j; r_i), \alpha^*(j; r_i)) \quad (7)$$

where δ is the Kronecker delta. When the squared difference metric $\ell(a, b) = (a - b)^2$ is used in (3), we use $e_l = \sqrt{L(\alpha; c(z), \mathcal{E})/(MN)}$ to characterize the error in arrival time as a consequence of misassociation.

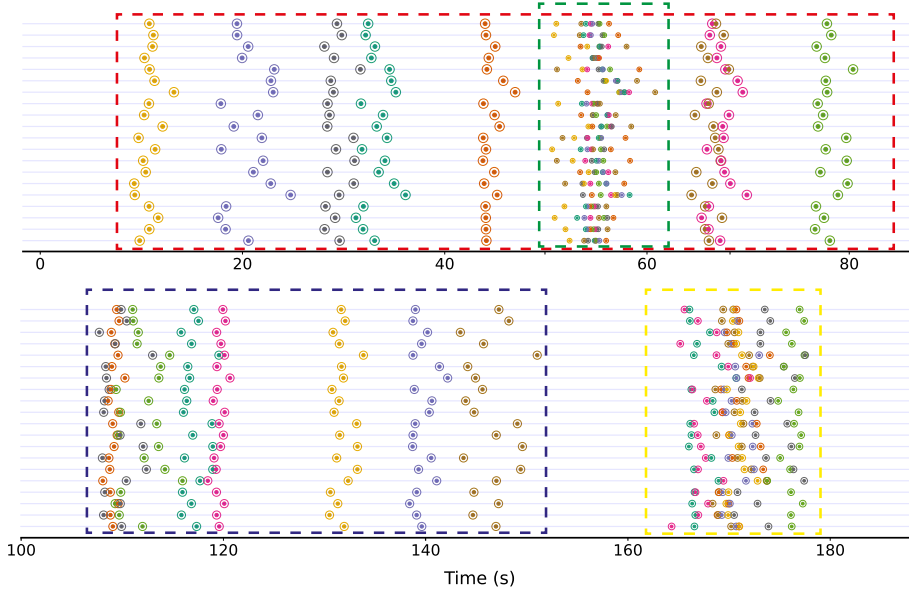


Figure 2: Phase association for different arrival rates / confusion factors. Each colored frame contains 8 sources recorded by 20 stations. Each horizontal line represents a stations, with colored circles representing arrivals. The inner circle color encodes the ground truth association; the outer circle color encodes association computed by HARPA. **Green:** CF = 0.88, ACC = 97.5%, $e_l = 0.04$ s; **yellow:** CF = 0.42, ACC = 98.8%, $e_l = 0.03$ s; **navy blue:** CF = 0.05, ACC = 100%, $e_l = 0.02$ s; (4) **red:** CF = 0.02, ACC = 100%, $e_l = 0.03$ s.

3 Method

3.1 Association without association

For a known wave speed and spatio-temporal source locations, and in the absence of error in travel time estimates, the optimal assignment α^* yields $L(\alpha^*) = 0$ in (2). This assignment can thus be obtained simply as

$$\alpha(j, r_i) = \arg \min_k \ell(T_c(s_j; r_i) + \tau_j, t_{i,k}). \quad (8)$$

Instead of directly addressing phase association, we first solve a seemingly harder (approximate)

joint recovery problem. We map the arrival times \mathcal{D}_i to a discrete probability measure

$$\rho_i = \frac{1}{M} \sum_{k=1}^M \mathbb{1}_{\{t_{i,k}\}} \quad (9)$$

which we regard as the ground truth probability measure. By “passing through the wave equation” we can similarly construct a discrete probability measure for any wave speed latent code z and earthquake sources with parameters \mathcal{E} ,

$$\rho_i^{\mathcal{E},z} = \frac{1}{M} \sum_{e_j \in \mathcal{E}} \mathbb{1}_{\{T(s_j, r_i, z) + \tau_j\}}, \quad (10)$$

We aim to align these two measures by minimizing their Wasserstein distance defined for $p \geq 1$ as

$$w_p(\rho_1, \rho_2) = \left(\inf_{\gamma \in \mathcal{C}(\rho_1, \rho_2)} \int |\theta_1 - \theta_2|^p \gamma(d\theta_1, d\theta_2) \right)^{1/p}. \quad (11)$$

In the case where some phase picks are missing or spurious picks are present, we define a loss for matching unbalanced arrivals based on sparsity-constrained optimal transport; a detailed description is given in Appendix E and results in Figure 9c. In the 1-dimensional discrete case this loss coincides with the Wasserstein loss of the unbalanced linear assignment.

The source locations and times can finally be estimated by optimizing the following loss (cf. Figure 3),

$$\begin{aligned} & \underset{\mathcal{E}, z}{\text{minimize}} \quad W(\mathcal{E}, z) \\ & \text{where} \quad \sum_{i=1}^N w_p(\rho_i^{\mathcal{E}, z}, \rho_i) \quad \text{and} \quad \rho_i^{\mathcal{E}, z} = \frac{1}{M} \sum_{e_j \in \mathcal{E}} \mathbb{1}_{\{T(s_j, z; r_i) + \tau_j\}}. \end{aligned} \quad (12)$$

What this passing to measures affords us is invariance to permutations of arrivals. In other words, it removes the need for association. We can relate (12) to (2) where we explicitly sought the optimal assignment α^* as follows. In the noiseless setting, we have

$$\rho_i^{\mathcal{E}^*, z^*} = \frac{1}{M} \sum_k \mathbb{1}_{\{T_{c^*}(s_{(\alpha^*)}^*; r_i)^{-1}(k; r_i); r_i) + \tau_{(\alpha^*)}^*; r_i\}},$$

where \mathcal{E}^*, z^* on the left hand side are the solution of (12) while $c^*, \alpha^*, (s^*, \tau^*)$ on the right hand side are the solution of (2). After obtaining $\mathcal{E}^* = (s^*, \tau^*)$ from (12), we can find α^* by solving LSAP directly, or by using only s^* without τ^* by solving the TDoA problem as in (4)).

We assume that earthquakes are well-approximated by point sources which are distributed volumetrically so that we obtain sufficiently rich data. These conditions are satisfied in reality with events occurring close to ensembles of faults (or fractures) at varying orientations, or in “clouds” [11, 41].

3.1.1 Latent representation of wave speeds and travel time neural fields

The complexity of solving (12) strongly depends on the complexity of computing the travel time function $T(s, z; r)$. For a given wave speed (or its latent code z) we can use a standard numerical solver to obtain the value of T at a desired set of points.

This, however, poses major challenges: numerical solvers work on grids or meshes; we would like to use continuous optimization to optimize source locations which is far from straightforward with

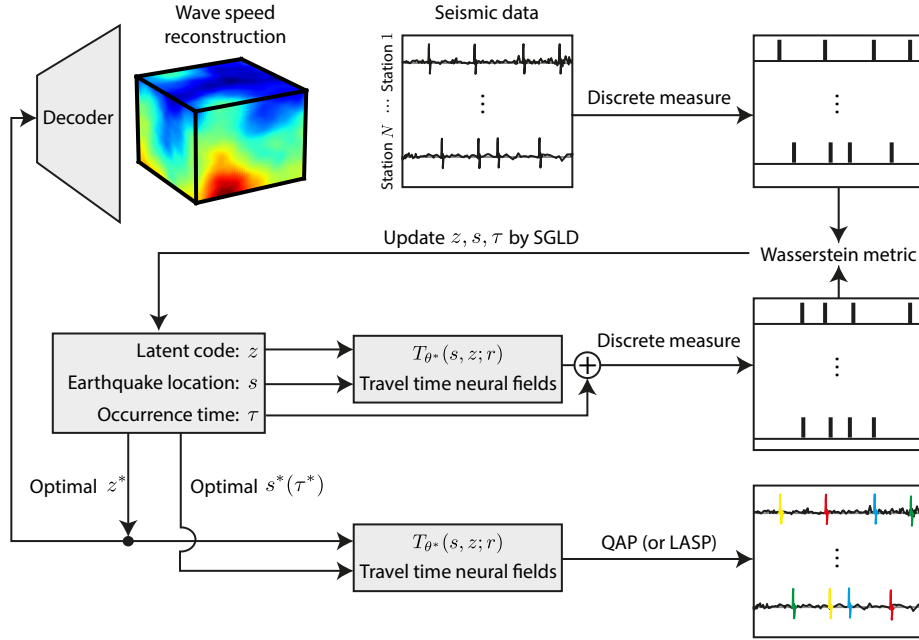


Figure 3: Diagram of HARPA’s association pipeline.

a fixed discrete grid. Even if we could circumvent the grid issue, taking gradients to use differential optimization would require us to differentiate T both with respect to the source location and with respect to the latent code z . And even if we implement it, the computational complexity of differentiating through an iterative solver would result in an exceedingly slow method.

The way we resolve this conundrum in HARPA is as follows: We first use a deep autoencoder to build a low-dimensional latent representation of a set of complex wave speeds; see Section 4 and Figure 4. Next, we use the fast marching method as implemented in `scikit-fmm` to compute the travel times between a fixed set of receivers and sources at each possible mesh node. The final and key step is then to fit a neural field (also known as an implicit neural representation) to the travel time data [24, 33]. We use a neural network T_θ with weights θ and periodic activation functions [33] which ensures that travel times and their derivatives with respect to source locations and wave speed latent codes can be efficiently evaluated at continuous coordinates. We train T_θ so that $T_{\theta^*}(s, z; r) \approx T(s, z; r)$ by fitting the travel time at a discrete set of grid points in space,

$$\theta^* = \arg \min_{\theta} \sum_{z \in \mathcal{Z}, s \in \mathcal{S}, r \in \mathcal{R}} (T(s, z; r) - T_\theta(s, z; r))^2, \quad (13)$$

where \mathcal{Z} denotes the set of sampled wave speeds (that is to say, their corresponding latent codes), \mathcal{S} represents the set of coordinates in the spatial domain (typically chosen as a grid), and $T(s, z; r)$ is pre-computed using a numerical solver. The latent travel time neural field, which mimics the real travel time function, provides a continuous representation of the travel time which is differentiable with respect to both s and z , thus enabling gradient-based optimization.

3.1.2 Solving the non-convex optimization problem

The Wasserstein loss in (12) is differentiable with respect to both z and \mathcal{E} but it is not convex which means that local gradient-based optimization may converge to local minima. The total number of

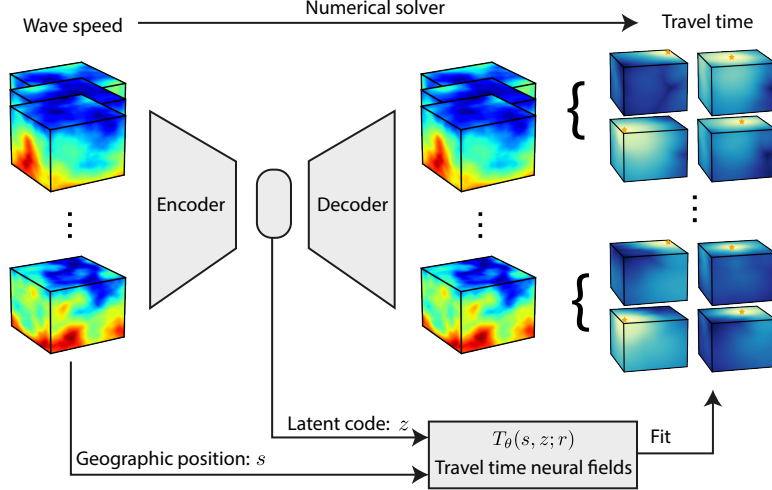


Figure 4: Diagram of the wave speed autoencoder and the travel time neural field.

parameters, $(3 + 1) \times N + L$, is small compared with common deep neural networks so there is no reason to expect that these local minima are benign. Indeed, as shown in Appendix A, we observe empirically that stochastic gradient descent (SGD) often converges to poor local minima. This issue can be addressed by Monte Carlo sampling methods, but this would be prohibitively slow in our setting.

It is natural to try and benefit from the favorable aspects of sampling methods and SGD by combining them in an iterative optimizer. A notable example of this group of algorithms, which we employ in HARPA, is stochastic gradient Langevin dynamics (SGLD) [37], which can be viewed either as a mini-batch variant of Langevin dynamics or as a noisy SGD. The global convergence of Langevin dynamics can be leveraged to locate the globally-optimal earthquake and wave speed parameters which approximate their corresponding ground truth values, while benefiting from fast convergence rates [21, 40]; here the (relatively) small number of parameters helps. At each step, SGLD iterates according to

$$\begin{aligned} z &\leftarrow z - \eta \widehat{\nabla_z W} + \sqrt{2\eta}\epsilon\xi_z, \\ s &\leftarrow s - \eta \widehat{\nabla_s W} + \sqrt{2\eta}\epsilon\xi_s, \\ \tau &\leftarrow \tau - \eta \widehat{\nabla_\tau W} + \sqrt{2\eta}\epsilon\xi_\tau, \end{aligned} \tag{14}$$

where η is the step size, and $\widehat{\nabla W}$ is an unbiased estimator of gradient ∇W , specifically a mini-batch sum in (12). The parameter ϵ modulates the amplitude of noise; ξ_z , ξ_s , and ξ_τ are standard normal vectors independently drawn across different iterations from a Gaussian distribution with mean zero and variance one.

4 Experiments and results

We now present a suite of results from computer experiments. In Section 4.1 we first test the limits of HARPA on a challenging set of unknown wave speeds in terms of the numbers of sources and receivers and show successful association in a variety of settings. We work with both known and unknown wave speeds. In Section 4.2 we apply HARPA to realistic wave speed models derived from the SEG / EAGE 3-D overthrust model [3] which come from a different distribution than the one used to train the latent wave speed model and show that the proposed method is robust to such

perturbations. Finally, in Section 4.3 we demonstrate robustness to spurious and missing phase picks.

4.1 Association via joint recovery

We simulate wave propagation in a region of size $100 \text{ km} \times 100 \text{ km} \times 100 \text{ km}$, with wave speeds ranging from 5 km/s to 25 km/s . We assume that the distribution of earthquake locations is uniformly random inside this volume and that the stations are uniformly distributed on the surface

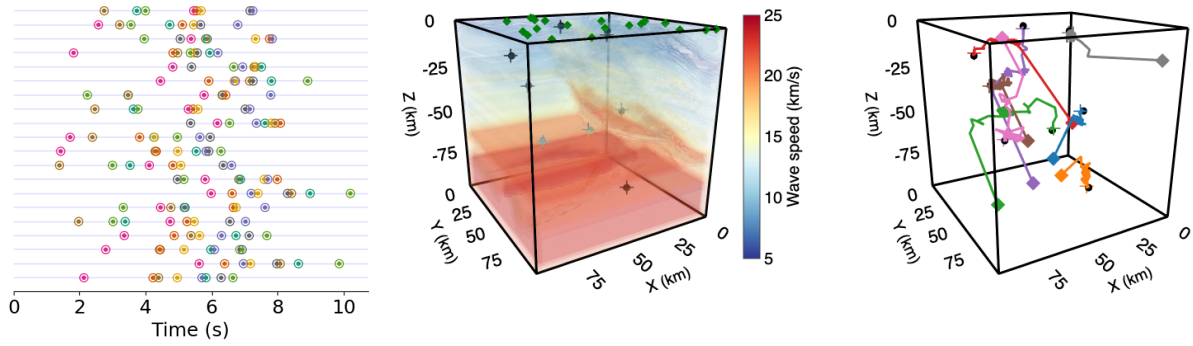


Figure 5: Association results for 8 sources, 20 stations and $\text{CF} = 0.93$ with SEG/EAGE 3-D overthrust model as the known wave speed. HARPA achieves $\text{ACC} = 95.0\%$ and $e_l = 0.03$ s. **Left:** each horizontal line represents the arrivals at one station. Inner circles show the correct association and outer circles show the association results of HARPA. **Middle:** color corresponds to the wave speed; green diamonds, black crosses, and black circles represent station locations, predicted earthquake locations, and ground truth earthquake locations, respectively. **Right:** source trajectories during SGLD-based learning; diamond markers are initial locations, cross markers stopping points after 100 epochs.

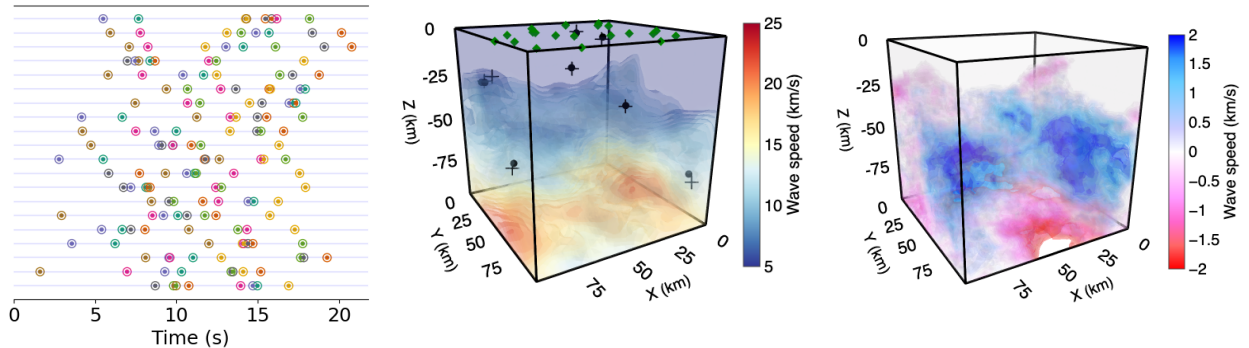


Figure 6: Association results for 8 sources, 20 stations and $\text{CF} = 0.94$ with unknown wave speed. HARPA achieves $\text{ACC} = 91.3\%$ and $e_l = 0.07$ s. **Left:** each horizontal line represents the arrivals at one station. Inner circles show the correct association and outer circles show the association results of HARPA. **Middle:** wave speed recovered by HARPA. **Right:** difference between the recovered and ground truth wave speed. Definitions of symbols are as in Figure 5.

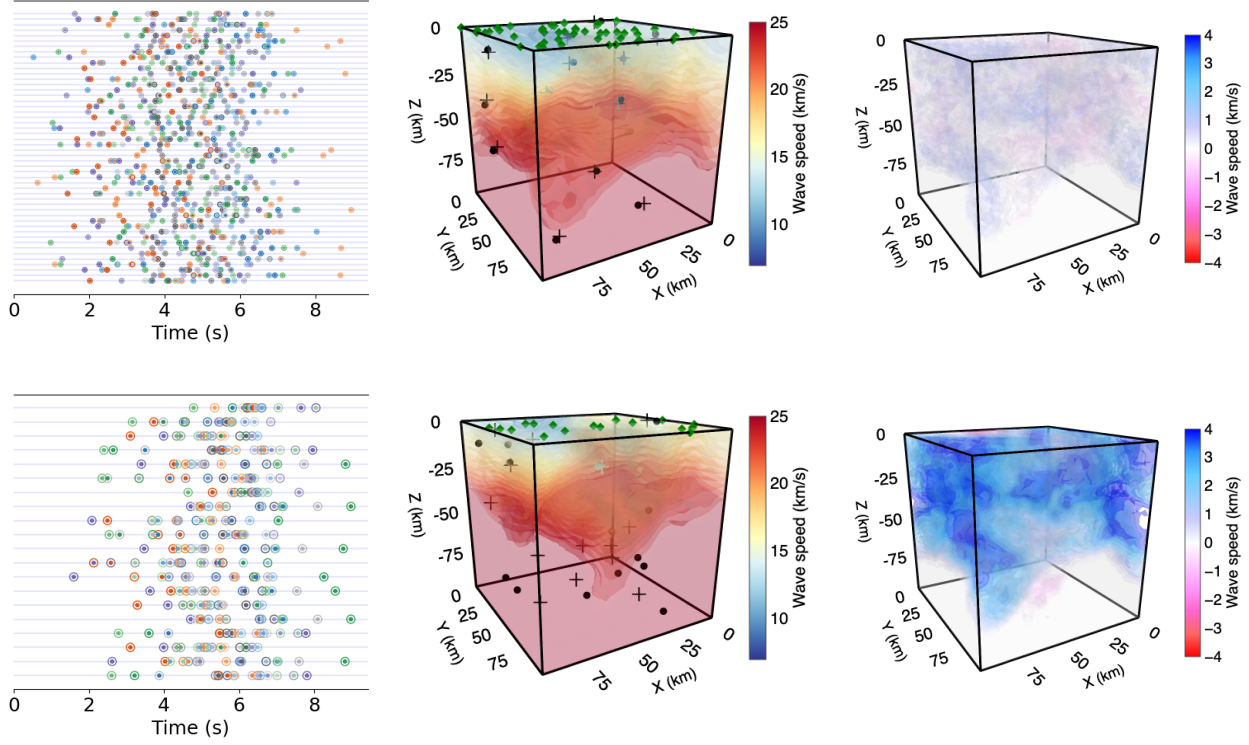


Figure 7: Association results for 16 sources with 20 and 50 stations. **Top row (50 stations):** $ACC = 72.0\%$, $e_l = 0.10$ s, $CF = 0.98$. **Bottom row (20 stations):** $ACC = 28.4\%$, $e_l = 0.29$ s, $CF = 0.90$. Symbols and encoding are as in Figure 6.

at $z = 0$. Occurrence times of earthquakes, τ_j , are uniformly distributed on the interval $[0, \tau_{\max}]$. The confusion factor CF can be modulated by changing τ_{\max} ; a larger τ_{\max} makes the association easier for a fixed number of sources and stations. Figure 2 illustrates the varying levels of difficulty in association for different CF.

4.1.1 Known wave speed

In the known wave speed experiment, we used SEG/EAGE 3-D overthrust model [3] (left plot in Figure 1), rescaled to our experimental volume. It is remarkable that despite the complexity of the wave speed HARPA achieves near 100% association accuracy, even in the most challenging cases with many overlapping arrivals (green window in Figure 2) where the ordinal number of arrivals is completely different from station to station. Another experiment with a known wave speed experiment is shown in Figure 10.

4.1.2 Unknown wave speed

We constructed a dataset of synthetic wave speeds by superimposing realizations of a Gaussian random field onto a vertical gradient wave speed (details in Appendix B). This is a challenging setting for association which exhibits strong spatial variation and a large five-fold dynamic range of wave speeds, typically between 5 km/s and 25 km/s. The test wave speed in this experiment comes from the same distribution (it is not included in the training set). In Appendix D we also report

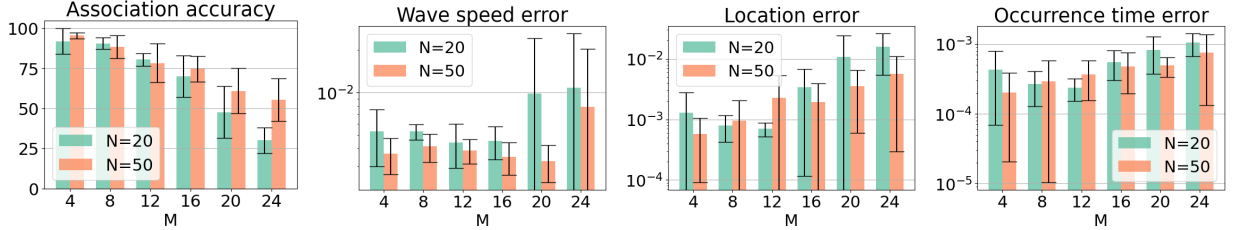


Figure 8: Evaluation of HARPA with varying number of stations (N) and sources (M)).

Left to right, the four panels illustrate the impact on (a) association accuracy, (b) relative wave speed error, (c) relative earthquake location error, and (d) relative earthquake occurrence time error. Bars show the mean of 10 independent runs; error bars indicate standard deviation. For efficiency we used a smaller and simpler dataset, with up to 2 random fields compared to 3 in other experiments and the latent dimension $L = 4$ instead of $L = 6$ (See Appendix C for the data generation protocol). The mean CF is 0.80.

results for a different distribution of wave speeds obtained as random Gaussian perturbations.

Figure 6 shows results for a setting with $CF = 0.94$. The pointwise error between the true and the recovered wave speeds is everywhere below 2 km/s; the corresponding root-mean-squared error (RMSE) is 0.78 km/s; the RMSE in earthquake spatial locations is 3.48 km. This is achieved with wave speeds ranging from 5 km/s to 25 km/s within a $100 \text{ km} \times 100 \text{ km} \times 100 \text{ km}$ volume. As a result of this accurate recovery, the accuracy of the subsequent association is 91.3%. As we can see from the left panel in Figure 6, HARPA achieves this high association accuracy in spite of the fact that the waves arrive at the different stations in completely different sequences and are packed close together in time; existing method simply do not work in this regime. The only association errors made by HARPA are for the picks which are almost entirely overlapped and which are confused with their neighbors.

In Figure 7 we test the performance of HARPA in handling a high number of simultaneous earthquake events. We perform association for 16 arrivals occurring in less than half the time from Figure 6. We see that with 50 stations we can nonetheless obtain an accurate association, again with most of the confused arrivals being close in time. When the number of stations decreases to 20 the association accuracy deteriorates.

Interestingly, while additional stations and sources might initially cause confusion in arrival times and contribute to erroneous association, they enhance wave speed reconstruction. For example, in the top row in Figure 7, even though the earthquake locations and the wave speed are accurately recovered (with mean errors of 3.18 km and 1.94 km/s), the misassociations are inevitable due to completely overlapping arrivals. Increasing the number of stations and sources provides additional travel time information, ultimately benefitting wave speed reconstruction. More results for different numbers of stations and events are shown in Figure 8.

4.2 Distorted and out-of-distribution wave speeds

Next, we study the robustness of the proposed method in situations where the true wave speed comes from a different distribution than the one used to train HARPA’s travel time neural field. In other words, the ground truth wave speed is markedly different from any wave speed seen by the autoencoder, both qualitatively and quantitatively.

In the “distortion” experiment (Figure 9a), we use the same fixed wave speed c_0 used in Section 4.1.1 to learn travel time neural fields, while the true (test) wave speed is a linear interpolation

between c_0 and another fixed wave speed c_1 , $c^* = (1 - p_d)c_0 + p_d c_1$; when $p_d = 0$, there is no model distortion between training and deployment. In the “out of distribution” experiment (Figure 9b), we use the travel time neural field for a wave speed distribution described in Section 4.1.2. The true (test) wave speed is generated according to $c^* = (1 - p_o)c_2 + p_o c_0$, where c_2 is a wave speed randomly sampled in-distribution and c_0 is the out-of-distribution perturbation. A large p_o means that c^* is far from the training wave speed distribution. In either case we let c_0 be the SEG/EAGE 3-D overthrust model, qualitatively rather different from Gaussian random field samples c_1 and c_2 .

We highlight that, compared with the fixed wave speed experiment in Figure 9a, the generative model in HARPA makes the recovery much more robust. For small CF, the association accuracy (orange heatmap) is still very high even though the test wave speed is far out of distribution. It is further worth noting that in cases where the arrival sequence from different events is similar at all stations (small CF), accurate wave speed recovery and source localization are not necessary for a good association. This observation aligns with previous studies on the low-rate regime where fixed wave speed models which only vary in the depth coordinate yield good association performance.

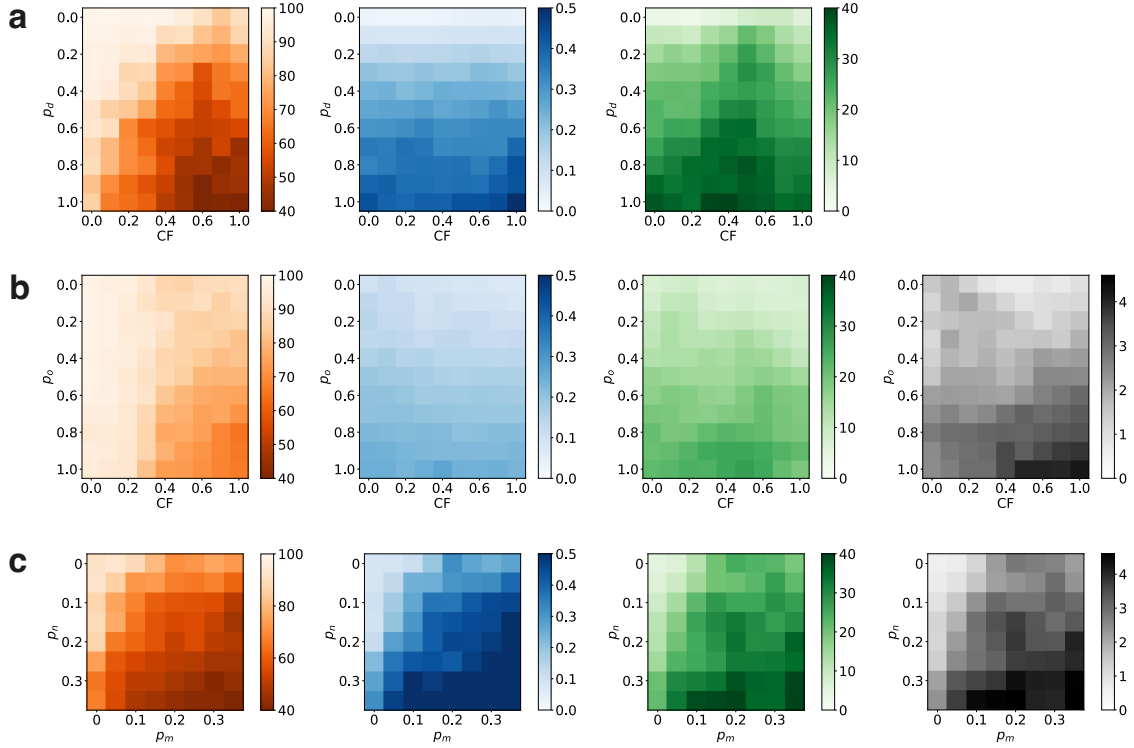


Figure 9: Robustness of HARPA under distortion and noise quantified by association accuracy ACC (orange), signal matching error e_l in seconds (blue), earthquake location error in km (green) and mean wave speed reconstruction error in km/s (grey), as a function of (a) wave speed distortion (p_d) and the confusion factor CF; (b) excursion from training distribution (p_o) and confusion factor CF; (c) fraction of noisy (p_n) and missing (p_m) picks. All values are averages of 20 trials. In (c), the ACC and e_l are determined by comparison with the original noiseless picks and the average CF is 0.80; the setting in other panels is as in Figure 8.

4.3 Spurious and missing picks

When working with real seismograms it may happen that some picks are missing, for example because a station is too far from the source. Conversely, the peak picking algorithm may make spurious detections. We test the performance of HARPA to these types of error. In Figure 9c, we arbitrarily eliminate a p_m fraction of arrivals at each station and introduce an additional p_n fraction of random picks. When $p_n > p_m$, the number of picks at each station is typically larger than the number of events we are searching for. Conversely, when $p_n < p_m$, the number of picks at each station is typically smaller than the number of events we are searching for. We see in the figure that small-to-moderate ratios of noisy and missing picks do not significantly hurt the association accuracy (orange heat map in Figure 9c) even when $\text{CF} = 0.80$.

5 Discussion

Existing association algorithms operate under the assumption that the wave speed is approximately known and are applied in low-rate settings where the order of arrivals of waves from the different events coincides at all stations [44]. A major challenge addressed by these methods is to sieve out spurious and missing arrivals which hamper association.

We explore a different regime where the arrivals are extremely dense in occurrence time, the ordinal number of arrival at a station is a priori meaningless, and the wave speed is unknown. This regime is of great interest for earthquake monitoring but inaccessible to existing methods; see for example the density and mixing-up of arrivals that we successfully associate in Figure 8, notwithstanding the unknown wave speed. The fact that we can still obtain accurate association in situations of this complexity opens up new domains of application. Quoting from [1], “a comprehensive study of microseismicity can provide a valuable description of the geological medium properties and earthquake related processes in the investigated crustal volumes, such as for instance the identification and geometrical characterization of active fault structures.”.

Indeed, taming microseismicity would allow us to monitor the changes in time of the elastic material properties. One case in point is monitoring sustainable energy production facilities [12]; another is understanding fault activity in earthquakes caused by unconventional hydrocarbon development; as Park and coauthors write [28], “Microearthquake activity can illuminate otherwise unknown faults, particularly when events are detected down to low magnitudes and are located precisely.”

From a high-level perspective there are two reasons that make our proof of concept, HARPA, work. The first is that we take an inverse problems perspective and approximately recover continuous unknowns by interpreting the observed data as a probability measure. Indeed, in situations of such complexity it is unlikely that statistical filtering methods can work well without explicitly using some model of wave propagation. Since we still only obtain (coarse) approximations of the relevant parameters we cannot claim to solve the full travel time tomography problem, but it is conceivable that the resulting association and the approximate locations and wave speeds could be used as a warm start for a linearized or iterative method [10].

The second reason is that we leverage a body of theoretical and engineering developments from deep learning: efficient optimal transport routines, neural fields, automatic differentiation, generative models, stochastic optimization and sampling, are all essential components of HARPA.

Computer experiments show that HARPA is robust to moderate wave speed distribution distortion and noisy arrival picks. A fully practical field deployment, however, requires additional work on robustness to spurious and missing picks which may be achieved through a judicious use of sparse unbalanced optimal transport. Another exciting possibility is to use multiple temporal

windows instead of a single one and thus effectively work with a very large number of events. This is straightforward in principle but the current bottleneck is computational efficiency. Faster optimization algorithms would open up the possibility to work with general rather than low-dimensional wave speed models and ultimately perform ab initio nonlinear travel time tomography with unknown sources.

References

- [1] Guido Maria Adinolfi, Grazia De Landro, Matteo Picozzi, Francesco Carotenuto, Alessandro Caruso, Sahar Nazeri, Simona Colombelli, Stefania Tarantino, Titouan Muzellec, Antonio Emolo, and et al., *Comprehensive study of micro-seismicity by using an automatic monitoring platform*, *Frontiers in Earth Science* **11** (2023), 1073684.
- [2] Ravindra K Ahuja, James B Orlin, and Ashish Tiwari, *A greedy genetic algorithm for the quadratic assignment problem*, *Computers & Operations Research* **27** (2000), no. 10, 917–934.
- [3] Fred Aminzadeh, P Weimer, and T Davis, *3-d salt and overthrust seismic models*, *Studies in Geology* **42** (1996), 247–256.
- [4] James M Bardeen, JR Bond, Nick Kaiser, and AS Szalay, *The statistics of peaks of Gaussian random fields*, *Astrophysical Journal, Part 1* (ISSN 0004-637X), vol. 304, May 1, 1986, p. 15-61. SERC-supported research. **304** (1986), 15–61.
- [5] Una Benlic and Jin-Kao Hao, *Breakout local search for the quadratic assignment problem*, *Applied Mathematics and Computation* **219** (2013), no. 9, 4800–4815.
- [6] Rainer Burkard, Mauro Dell’Amico, and Silvano Martello, *Assignment problems: revised reprint*, SIAM, 2012.
- [7] Maarten V de Hoop, Joonas Ilmavirta, Matti Lassas, and Teemu Saksala, *Stable reconstruction of simple Riemannian manifolds from unknown interior sources*, arXiv preprint arXiv:2102.11799 (2021).
- [8] Ivan Dokmanić, Reza Parhizkar, Andreas Walther, Yue M Lu, and Martin Vetterli, *Acoustic echoes reveal room shape*, *Proceedings of the National Academy of Sciences* **110** (2013), no. 30, 12186–12191.
- [9] John Dubinski and RG Carlberg, *The structure of cold dark matter halos*, *Astrophysical Journal, Part 1* (ISSN 0004-637X), vol. 378, Sept. 10, 1991, p. 496-503. **378** (1991), 496–503.
- [10] Hongjian Fang, Robert D Van Der Hilst, Maarten V de Hoop, Konik Kothari, Sidharth Gupta, and Ivan Dokmanić, *Parsimonious seismic tomography with Poisson Voronoi projections: methodology and validation*, *Seismological Research Letters* **91** (2020), no. 1, 343–355.
- [11] Stanislav Glubokovskikh, Christopher S Sherman, Joseph P Morris, and David L Alumbaugh, *Transforming microseismic clouds into near real-time visualization of the growing hydraulic fracture*, *Geophysical Journal International* (2023), ggad248.
- [12] Francesco Grigoli, John F Clinton, Tobias Diehl, Philipp Kaestli, Luca Scarabello, Thorbjorg Agustsdottir, Sigridur Kristjansdottir, Rognvaldur Magnusson, Christopher J Bean, Marco Broccardo, and et al., *Monitoring microseismicity of the Hengill Geothermal Field in Iceland*, *Scientific Data* **9** (2022), no. 1, 220.

- [13] Shuai Huang and Ivan Dokmanić, *Reconstructing point sets from distance distributions*, IEEE Transactions on Signal Processing **69** (2021), 1811–1827.
- [14] Jaromír Jansky, Vladimir Plicka, and Leo Eisner, *Feasibility of joint 1d velocity model and event location inversion by the neighbourhood algorithm*, Geophysical Prospecting **58** (2010), no. 2, 229–234.
- [15] Maurice G Kendall, *A new measure of rank correlation*, Biometrika **30** (1938), no. 1/2, 81–93.
- [16] Tjalling C Koopmans and Martin Beckmann, *Assignment problems and the location of economic activities*, Econometrica: Journal of the Econometric Society (1957), 53–76.
- [17] Chunyuan Li, Changyou Chen, David Carlson, and Lawrence Carin, *Preconditioned stochastic gradient Langevin dynamics for deep neural networks*, Proceedings of the AAAI Conference on Artificial Intelligence, 2016.
- [18] Zhuwen Li, Qifeng Chen, and Vladlen Koltun, *Combinatorial optimization with graph convolutional networks and guided tree search*, Advances in Neural Information Processing Systems **31** (2018).
- [19] Min Liu, Miao Zhang, Weiqiang Zhu, William L Ellsworth, and Hongyi Li, *Rapid characterization of the July 2019 Ridgecrest, California, earthquake sequence from raw seismic data using machine-learning phase picker*, Geophysical Research Letters **47** (2020), no. 4, e2019GL086189.
- [20] Tianlin Liu, Joan Puigcerver, and Mathieu Blondel, *Sparsity-constrained optimal transport*, International Conference on Learning Representations, 2023.
- [21] Yi-An Ma, Yuansi Chen, Chi Jin, Nicolas Flammarion, and Michael I Jordan, *Sampling can be faster than optimization*, Proceedings of the National Academy of Sciences **116** (2019), no. 42, 20881–20885.
- [22] Ian W McBrearty and Gregory C Beroza, *Earthquake phase association with graph neural networks*, Bulletin of the Seismological Society of America (2023).
- [23] Ian W McBrearty, Joan Gomberg, Andrew A Delorey, and Paul A Johnson, *Earthquake arrival association with backprojection and graph theory*, Bulletin of the Seismological Society of America **109** (2019), no. 6, 2510–2531.
- [24] Ben Mildenhall, Pratul P Srinivasan, Matthew Tancik, Jonathan T Barron, Ravi Ramamoorthi, and Ren Ng, *Nerf: Representing scenes as neural radiance fields for view synthesis*, Communications of the ACM **65** (2021), no. 1, 99–106.
- [25] Peter Mora, Gabriele Morra, and David A Yuen, *Models of plate tectonics with the Lattice Boltzmann Method*, Artificial Intelligence in Geosciences **4** (2023), 47–58.
- [26] Alex Nowak, Soledad Villar, Afonso S Bandeira, and Joan Bruna, *Revised note on learning quadratic assignment with graph neural networks*, 2018 IEEE Data Science Workshop (DSW), 2018, pp. 1–5.
- [27] Panos M Pardalos, Henry Wolkowicz, et al., *Quadratic assignment and related problems: Discrete workshop, may 20-21, 1993*, Vol. 16, American Mathematical Soc., 1994.
- [28] Yongsoo Park, Gregory C Beroza, and William L Ellsworth, *Basement fault activation before larger earthquakes in oklahoma and kansas*, The Seismic Record **2** (2022), no. 3, 197–206.

[29] Zachary E. Ross, Benjamín Idini, Zhe Jia, Oliver L. Stephenson, Minyan Zhong, Xin Wang, Zhongwen Zhan, Mark Simons, Eric J. Fielding, Sang-Ho Yun, Egill Hauksson, Angelyn W. Moore, Zhen Liu, and Jungkyo Jung, *Hierarchical interlocked orthogonal faulting in the 2019 Ridgecrest earthquake sequence*, *Science* **366** (2019), no. 6463, 346–351.

[30] Zachary E Ross, Yisong Yue, Men-Andrin Meier, Egill Hauksson, and Thomas H Heaton, *Phaselink: A deep learning approach to seismic phase association*, *Journal of Geophysical Research: Solid Earth* **124** (2019), no. 1, 856–869.

[31] Zachary E Ross, Weiqiang Zhu, and Kamyar Azizzadenesheli, *Neural mixture model association of seismic phases*, arXiv preprint arXiv:2301.02597 (2023).

[32] MH Shahnas, DA Yuen, and RN Pysklywec, *Inverse problems in geodynamics using machine learning algorithms*, *Journal of Geophysical Research: Solid Earth* **123** (2018), no. 1, 296–310.

[33] Vincent Sitzmann, Julien Martel, Alexander Bergman, David Lindell, and Gordon Wetzstein, *Implicit neural representations with periodic activation functions*, *Advances in Neural Information Processing Systems* **33** (2020), 7462–7473.

[34] Chao Song, Tariq Alkhalifah, and Zedong Wu, *Microseismic event estimation and velocity analysis based on a source-focusing function*, *Geophysics* **84** (2019), no. 3, KS85–KS94.

[35] Junzhe Sun, Zhiguang Xue, Tieyuan Zhu, Sergey Fomel, and Norimitsu Nakata, *Full-waveform inversion of passive seismic data for sources and velocities*, *Seg international exposition and annual meeting, 2016*, pp. SEG–2016.

[36] Oriol Vinyals, Meire Fortunato, and Navdeep Jaitly, *Pointer networks*, *Advances in neural information processing systems* **28** (2015).

[37] Max Welling and Yee W Teh, *Bayesian learning via stochastic gradient Langevin dynamics*, *Proceedings of the 28th international conference on machine learning*, 2011, pp. 681–688.

[38] Ben Witten and Jeffrey Shragge, *Image-domain velocity inversion and event location for microseismic monitoring*, *Geophysics* **82** (2017), no. 5, KS71–KS83.

[39] Yiheng Xie, Towaki Takikawa, Shunsuke Saito, Or Litany, Shiqin Yan, Numair Khan, Federico Tombari, James Tompkin, Vincent Sitzmann, and Srinath Sridhar, *Neural fields in visual computing and beyond*, *Computer Graphics Forum*, 2022, pp. 641–676.

[40] Pan Xu, Jinghui Chen, Difan Zou, and Quanquan Gu, *Global convergence of Langevin dynamics based algorithms for nonconvex optimization*, *Advances in Neural Information Processing Systems* **31** (2018).

[41] Arno Zang, Volker Oye, Philippe Jousset, Nicholas Deichmann, Roland Gritto, Art McGarr, Ernest Majer, and David Bruhn, *Analysis of induced seismicity in geothermal reservoirs—an overview*, *Geothermics* **52** (2014), 6–21.

[42] Zhishuai Zhang, James W Rector, and Michael J Nava, *Simultaneous inversion of multiple microseismic data for event locations and velocity model with Bayesian inference*, *Geophysics* **82** (2017), no. 3, KS27–KS39.

[43] Weiqiang Zhu and Gregory C Beroza, *Phasenet: A deep-neural-network-based seismic arrival-time picking method*, *Geophysical Journal International* **216** (2019), no. 1, 261–273.

[44] Weiqiang Zhu, Ian W McBrearty, S Mostafa Mousavi, William L Ellsworth, and Gregory C Beroza, *Earthquake phase association using a Bayesian Gaussian mixture model*, Journal of Geophysical Research: Solid Earth **127** (2022), no. 5, e2021JB023249.

Appendices

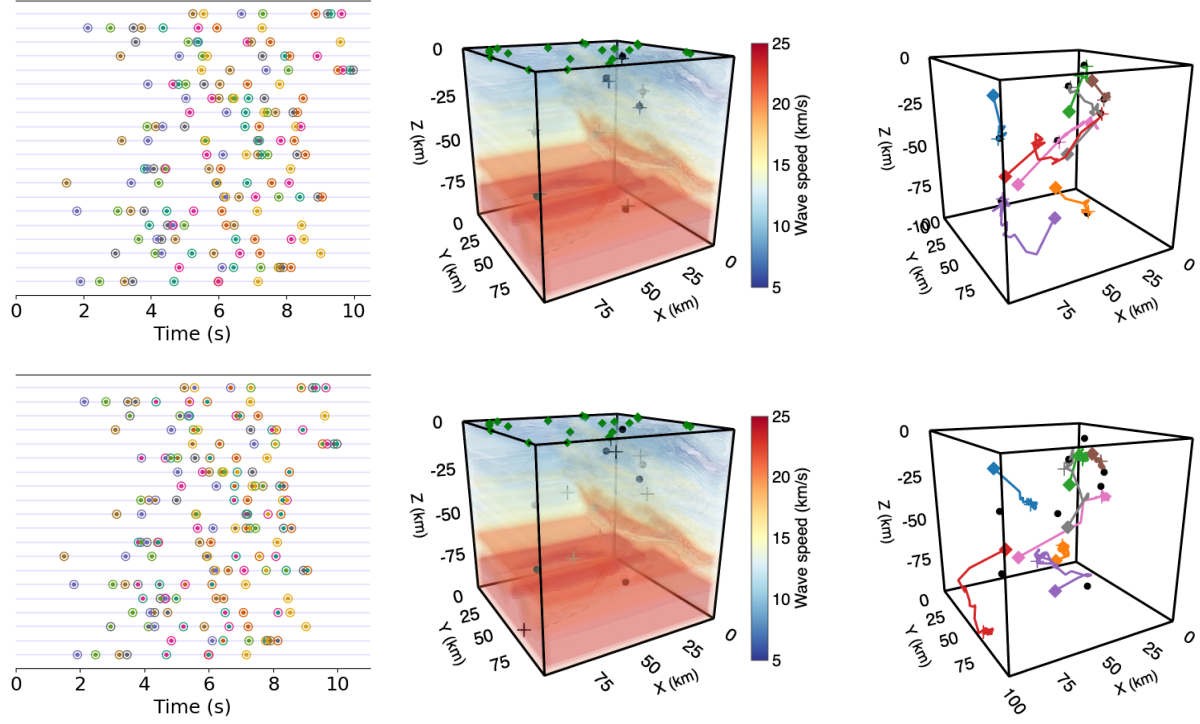


Figure 10: Association results for 8 sources, 20 stations and $CF = 0.85$ with SEG/EAGE 3-D overthrust model as the known wave speed. **Top row (SGLD):** $ACC = 92.5\%$, $e_l = 0.02s$. **Bottom row (SGD):** $ACC = 37.5\%$, $e_l = 0.59s$. Symbols and encoding are as in Figure 5; the right plot illustrates the source trajectories in the first 30 epochs of optimization.

A Comparison between SGD and SGLD

Here we show that due to non-convexity naive (stochastic) gradient descent converges to poor local minima, and that the issue is mitigated by SGLD. We compare SGD and SGLD on the fixed wave speed datasets described in Section 4. To visualize the optimization trajectory, we set the learning rate to 0.005 and $\epsilon = 0.0005$ (cf. (14)) for all epochs. Setting $\epsilon = 0$ reduces SGLD to SGD; the corresponding performance is reported in the second row in Figure 10. A visual comparison of the trajectories of source estimates during optimization (Figure 10, right) clearly shows that unlike SGD, SGLD easily escapes bad local minima.

B Gaussian random field dataset

In Figures 6, 7, and 8, the wave speeds are samples from the Gaussian random field dataset. To generate this low-dimensional wave speed dataset, we first created 20 three-dimensional Gaussian random fields as basis patterns in which the correlation is determined by scale-invariant power spectrum $P(k) \sim k^{-\alpha/2}$ [4,9]. We use $\alpha = 2.5$ in our experiments and rescale the pattern amplitudes

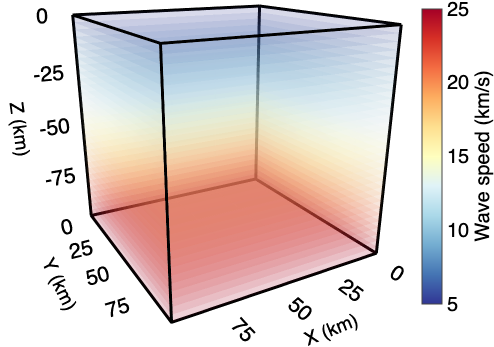


Figure 11: Background wave speed

to lie between 0 km/s and 15 km/s; representative samples are shown in Figure 12. For each sample, we randomly select up to 3 patterns and then add the selected patterns to a background wave speed (Figure 11) with weights drawn uniform at random in $[-1, 1]$. All wave speeds are clipped between 5 km/s and 25 km/s. In Figure 13 we show that this dataset is effectively modeled by a 3D convolutional autoencoder.

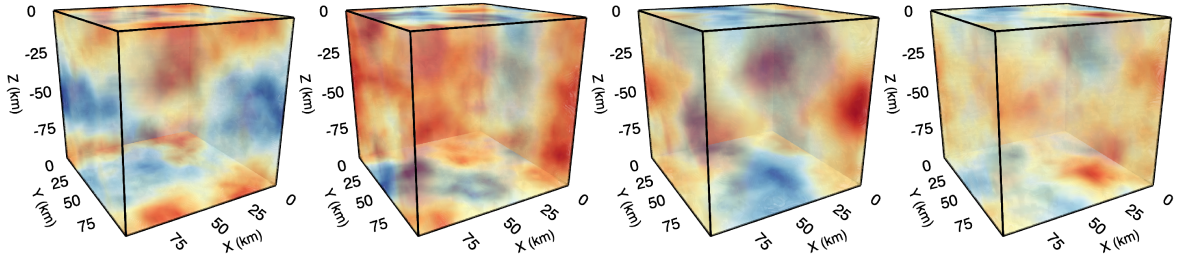


Figure 12: Four samples of the 3D Gaussian random fields with $\alpha = 2.5$.

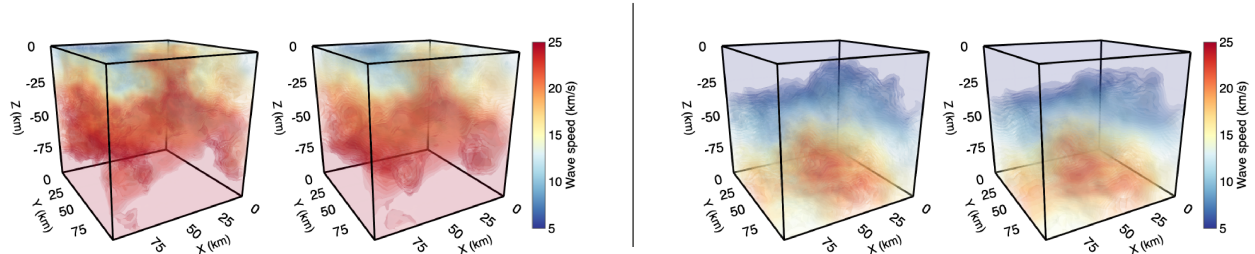


Figure 13: A comparison between two test wave speeds unseen at training time and the corresponding outputs from an auto-encoder with $L = 6$.

C Experimental details

C.1 Autoencoder

We discretize the wave speed into a $32 \times 32 \times 32$ cube, i.e., $c \in \mathbb{R}^{32 \times 32 \times 32}$, and use these cubic images to train a standard CNN autoencoder in `pytorch`. Due to the low-dimensional structure of the dataset, the autoencoder exhibits strong generalization when an appropriate dimension of the latent code $z \in \mathbb{R}^L$ is selected. A large L yields an autoencoder which accurately represents the wave speeds but also leads to slow SGLD inference. In our experiments we tested values of L between 3 and 6. The generalization performance of the autoencoder is illustrated in Figure 13.

The encoder comprises three 3D convolutional layers with a kernel size of 3^3 , a stride of 2, and padding of 1, each followed by a ReLU activation function. A subsequent linear layer generates the latent code z . Batch normalization is implemented between each layer. The decoder's architecture mirrors that of the encoder.

C.2 Training the travel time neural field

We compute the travel times from the receivers to all $32 \times 32 \times 32$ grid points for the aforementioned 10000 wave speeds using the fast marching method implemented in the `scikit-fmm` package.

We create a $(L+3)$ -dimensional feature vector for each grid point by concatenating its coordinate and the corresponding wave speed latent code, which are all scaled in $[0, 1]$ as the input to the neural field. We use a SIREN implicit network, a multilayer perceptron (MLP) with periodic activation functions [33]. The trained SIREN model not only provides accurate predictions of the travel time at the grid points but also immediately yields an interpolation at arbitrary continuous coordinates. The scaling constant w_0 in the sinusoidal activation function is important and depends on the grid scaling; we used $w_0 = 15$.

C.3 Optimization

We use the Python Optimal Transport (POT) package to compute the Wasserstein distance, with $p = 2$. We adopt the RMSProp-preconditioned version of the SGLD [17]. Both the learning rate (lr) and the noise factor (ϵ) are selected from $\{10^{-2}, 10^{-3}, 5 \times 10^{-3}, 10^{-4}\}$. The convergence speed depends on the choice of hyperparameters. To manage the exploration-exploitation trade-off, we reduce the learning rate (lr) to one-tenth of its original value once the loss decreases below a threshold l^* which is selected from $\{10^{-2}, 10^{-3}, 10^{-4}, 10^{-6}\}$. To speed up training, we implement an epoch threshold. If the loss fails to decrease below l^* before reaching this threshold, we reset all parameters and restart the training process. We set the maximum number of trials to 10. When τ_{\max} is very large or CF is close to 0, pre-training τ helps achieve faster convergence.

D Gaussian random perturbation dataset

In Figure 15 we report results on a different dataset in which we add between one and three random Gaussian perturbations on the background wave speed. These perturbations are defined as

$$\Delta c(x, y, z) = A \exp \left(-\frac{1}{2\sigma_x^2}(x - x_0)^2 - \frac{1}{2\sigma_y^2}(y - y_0)^2 - \frac{1}{2\sigma_z^2}(z - z_0)^2 \right),$$

where A is drawn uniformly at random from $[-25, 25]$, x_0, y_0, z_0 uniformly at random from $[0, 100]$ and $\sigma_x, \sigma_y, \sigma_z$ uniformly at random from $[10, 50]$; samples are shown Figure 14.

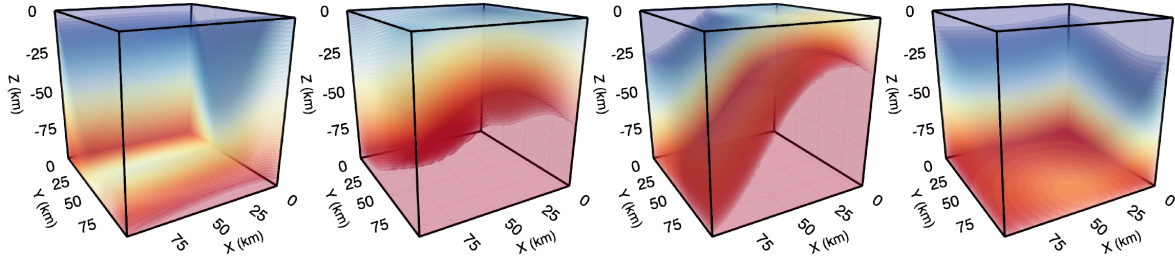


Figure 14: Four samples of wave speeds from the Gaussian perturbation dataset.

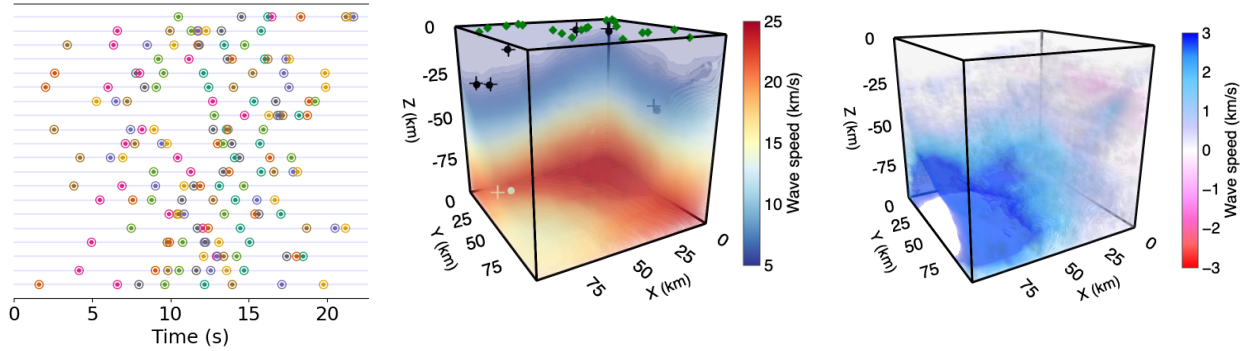


Figure 15: Association results for 8 sources, 20 stations and $CF = 0.79$ on Gaussian perturbation dataset. HARPA achieves $ACC = 96.3\%$ and $e_l = 0.02$ s. Symbols and encoding are as in Figure 6

E A Wasserstein misfit for unbalanced arrivals matching

We denote the cardinality of a finite set S by $|S|$ and let ρ_S be the uniform probability measure over its elements,

$$\rho_S = \frac{1}{|S|} \sum_{s \in S} \mathbb{1}_s.$$

We now consider two sets (of arrival times) A and B of possibly different cardinality. Without loss of generality, we assume $|A| \leq |B|$. We define a Wasserstein-like mismatch between these arrival sets as

$$\widehat{w}_p(A, B) = \min_{\tilde{B} \subseteq B, |\tilde{B}| = |A|} w_p(\rho_A, \rho_{\tilde{B}})$$

with w_p defined in Equation (11). This mismatch can be optimized by sparsity-constrained optimal transport [20]. In fact, in the 1D case it coincides with the loss of the unbalanced linear assignment problem

$$\overline{w}_p(A, B) = \min_{T \in \mathcal{T}_{|A|, |B|}} \frac{1}{|A|} \langle T, C \rangle,$$

where (arbitrarily vectorizing the elements of A and B as $a = (a_1, \dots, a_{|A|})$ and $b = (b_1, \dots, b_{|B|})$)

we used

$$\begin{aligned}\mathcal{T}_{|A|,|B|} &:= \left\{ T \in \{0,1\}^{|A| \times |B|} : T\mathbf{1}_{|B|} = \mathbf{1}_{|A|}, \ T^\top \mathbf{1}_{|B|} \leq \mathbf{1}_{|A|} \right\}, \\ C_{ij} &:= |a_i - b_j|^p.\end{aligned}\tag{15}$$

Here $\langle \cdot, \cdot \rangle$ denotes the Frobenius inner product and T the discrete transportation matrix. The all-ones vector of length K is denoted $\mathbf{1}_K$. For vectors $x, y \in \mathbb{R}^K$, the notation $x \leq y$ indicates that the inequality holds for all entries.